LETTERS
https://doi.org/10.1038/s41563-018-0149-7
nature materials

Two-dimensional itinerant ferromagnetism in atomically thin Fe_3GeTe_2

Zaiyao Fei[1,8], Bevin Huang[1,8], Paul Malinowski[1], Wenbo Wang[2], Tiancheng Song[1], Joshua Sanchez[1], Wang Yao[3], Di Xiao[4], Xiaoyang Zhu[5], Andrew F. May[6], Weida Wu[2], David H. Cobden[1], Jiun-Haw Chu[1]* and Xiaodong Xu[1,7]*

Discoveries of intrinsic two-dimensional (2D) ferromagnetism in van der Waals (vdW) crystals provide an interesting arena for studying fundamental 2D magnetism and devices that employ localized spins[1–4]. However, an exfoliable vdW material that exhibits intrinsic 2D itinerant magnetism remains elusive. Here we demonstrate that Fe_3GeTe_2 (FGT), an exfoliable vdW magnet, exhibits robust 2D ferromagnetism with strong perpendicular anisotropy when thinned down to a monolayer. Layer-number-dependent studies reveal a crossover from 3D to 2D Ising ferromagnetism for thicknesses less than 4 nm (five layers), accompanied by a fast drop of the Curie temperature (T_C) from 207 K to 130 K in the monolayer. For FGT flakes thicker than ~15 nm, a distinct magnetic behaviour emerges in an intermediate temperature range, which we show is due to the formation of labyrinthine domain patterns. Our work introduces an atomically thin ferromagnetic metal that could be useful for the study of controllable 2D itinerant ferromagnetism and for engineering spintronic vdW heterostructures[5].

Itinerant magnetism in metallic thin films has been investigated extensively for decades[6,7], including at the monolayer limit[6]. Such films serve as a testbed for the study of different aspects of 2D magnetism, for example, the critical behaviour and dimensional crossover of magnetic ordering[7], and are also important for technical applications, such as in memory devices[8]. The ultrathin films are typically prepared by molecular beam epitaxial (MBE) growth, and the magnetic behaviour is highly sensitive to the substrate surface and the resulting interface. Although this sensitivity imposes challenges in materials synthesis, it provides a method to engineer the magnetic properties of the film for magnetoelectronic applications that utilize exchange bias, giant/tunnelling magnetoresistance and spin torque[6,9]. Recently, the mechanical exfoliation of layered vdW crystals has emerged as a useful approach for realizing atomically thin insulating magnets and magnetic heterostructures. Although metallic ferromagnetism in vdW materials has been observed in MBE-grown monolayer VSe_2 (ref. [4]), no metallic ferromagnet that is exfoliable down to the monolayer limit has been demonstrated. One promising candidate is FGT (Fig. 1a).

Bulk crystalline FGT is an itinerant vdW ferromagnet with a reasonably high T_C of about 220–230 K (refs [10–14]). In addition to a large out-of-plane anisotropy[12], evidence for strong electron correlation effects[15] and Kondo lattice physics[16] has been seen recently. Encouragingly, first-principles calculations indicate that the large perpendicular magnetic anisotropy will persist down to a monolayer[17], which supports the possibility of sustaining long-range magnetic order in the 2D limit[18]. In fact, anomalous Hall effect (AHE) measurements on epitaxially grown FGT thin films[13] have revealed only a slight reduction of T_C from that of the bulk, which further supports the likelihood of anisotropy-stabilized long-range ferromagnetic order in ultrathin FGT flakes.

In this work, FGT flakes down to the monolayer limit were prepared by mechanical exfoliation from bulk crystals. The magnetic order was probed with both magnetotransport and Kerr rotation measurements. For the former, we cleaved FGT bulk crystals onto 285 nm SiO_2/Si substrates and patterned the resulting exfoliated thin flakes into Hall bars using electron beam lithography (Methods). Atomic force microscopy (AFM) measurements on a stepped FGT flake showed the layer step height to be ~0.8 nm (Fig. 1b), consistent with X-ray diffraction measurements[12]. The thinnest flake we could obtain by exfoliation onto SiO_2/Si was 4.8 nm, that is, six layers. For even thinner samples, we cleaved FGT bulk crystals onto a gold film evaporated on top of SiO_2/Si. As has been demonstrated with other materials, which include MoS_2 (refs [19–21]) and Bi_2Te_3 (ref. [19]), the gold substrate gives an increased yield of atomically thin flakes. However, the magnetic order in such samples can only be characterized by optical methods. Regardless, there is only a small difference in the magnetic response for FGT flakes thicker than 4 nm exfoliated on the two different substrates.

We first examine the magnetic properties of FGT thin flakes through magnetotransport measurements. Figure 1c shows the temperature-dependent longitudinal resistance, R_{xx}–T, of a representative 12 nm FGT Hall bar device (optical micrograph in upper-left inset). At ~210 K, the kinks in both R_{xx} and its first temperature derivative (lower-right inset) are characteristic of the established phase transition from paramagnetism to ferromagnetism. The Hall resistance, R_{xy} (Fig. 1d) shows rectangular hysteresis loops with near-vertical jumps at low temperatures as a function of external magnetic field, $\mu_0 H$, applied perpendicular to the sample plane, with the coercive field reaching 1 T at 2 K. This indicates the domination of the AHE with a single magnetic domain over the entire flake. Together with the large remanent R_{xy} at zero field, these are hallmarks of ferromagnetism with strong out-of-plane anisotropy. The remanent R_{xy} and coercive field vanishes at around 210 K, consistent with the kinks in Fig. 1c (Supplementary Section 1

[1]Department of Physics, University of Washington, Seattle, WA, USA. [2]Department of Physics and Astronomy, Rutgers University, Piscataway, NJ, USA. [3]Department of Physics and Center of Theoretical and Computational Physics, University of Hong Kong, Hong Kong, China. [4]Department of Physics, Carnegie Mellon University, Pittsburgh, PA, USA. [5]Department of Chemistry, Columbia University, New York, NY, USA. [6]Materials Science and Technology Division, Oak Ridge National Laboratory, Oak Ridge, TN, USA. [7]Department of Materials Science and Engineering, University of Washington, Seattle, WA, USA. [8]These authors contributed equally: Zaiyao Fei, Bevin Huang. *e-mail: jhchu@uw.edu; xuxd@uw.edu

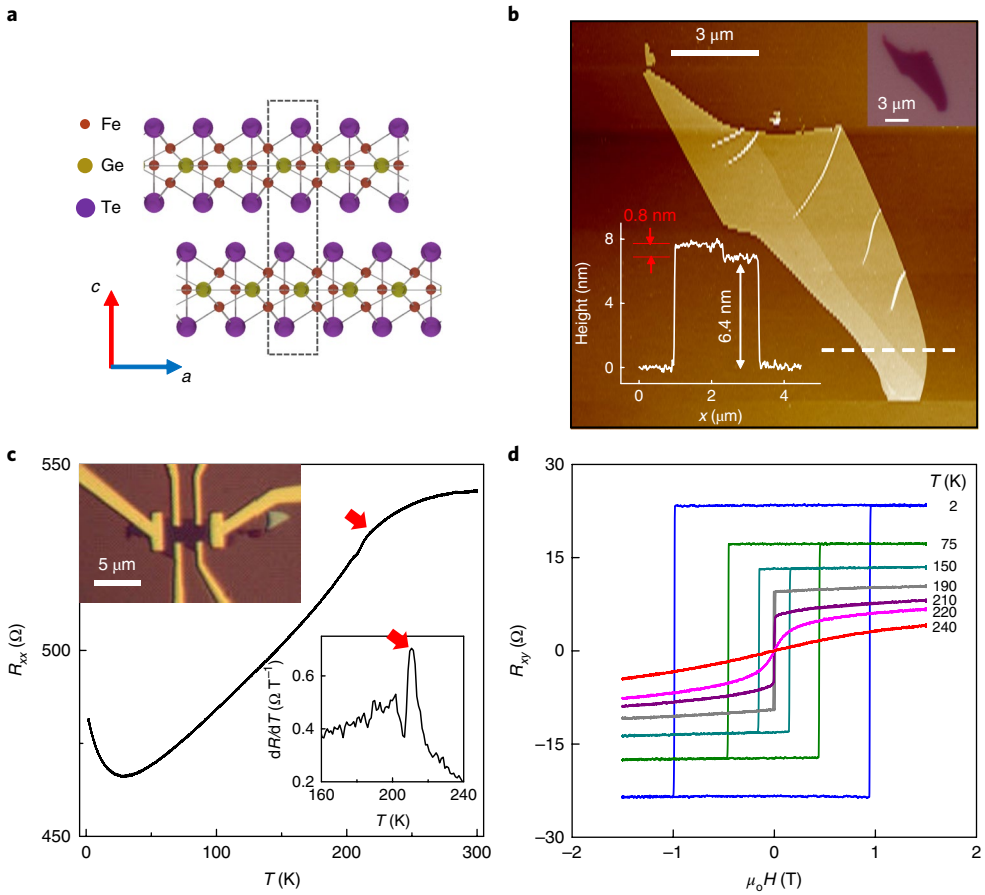

Fig. 1 | Structure and transport characterization of thin FGT flakes. a, Side view of the atomic lattice of bilayer FGT. The dashed rectangular box denotes the crystal unit cell. **b**, AFM image and optical image (upper right inset) of a representative thin FGT flake on 285 nm SiO_2. The lower-left inset shows a monolayer step of ~0.8 nm along the white dashed line. **c**, Temperature dependence of the longitudinal resistance of a representative FGT device (12 nm thick). The upper-left inset shows an optical image of the Hall bar device. The bottom-right inset shows the first derivative of the longitudinal resistance as a function of temperature. The red arrows show where the ferromagnetic–paramagnetic transition occurs. **d**, Temperature-dependent magnetic field (out-of-plane) sweeps of the Hall resistance measured on the 12 nm thick FGT device.

for additional magnetotransport measurements). These transport measurements show that the itinerant ferromagnetism exhibited in bulk crystals[10–12] and in MBE grown samples[13] persists in thin exfoliated FGT flakes.

To study truly 2D itinerant ferromagnetism, we investigated FGT flakes down to the monolayer limit on the gold substrates (Supplementary Fig. 2 contains optical and AFM images). We employed both polar reflective magnetic circular dichroism (RMCD) and the magneto-optical Kerr effect (MOKE) microscopy to examine the out-of-plane magnetic order (Methods). The magnetic field was applied perpendicular to the sample and the excitation laser was a 1 μW 633 nm HeNe laser with a spot size of 3 μm. Figure 2a shows the RMCD signal of a monolayer (false-colour optical micrograph in the inset) as $\mu_0 H$ was swept between −0.2 and 0.2 T at 78 K. Notably, ferromagnetism persists, as evidenced by the prominent hysteresis seen here. A spatial map of the RMCD intensity at 0.2 T (Fig. 2b) also reveals the magnetization to be uniform across the entire monolayer flake.

Figure 2c shows RMCD measurements as a function of magnetic field for several fixed temperatures. As the temperature increases, the hysteresis loop shrinks, disappearing at about 130 K. The same behaviour was observed for all four monolayers measured and implies that T_C, the temperature at which the ferromagnetic phase transitions to the paramagnetic phase, is about 130 K for monolayers. The T_C can also be extracted from a temperature dependence of the remanent RMCD signal (blue circles in Fig. 3). The onset of magnetization in the monolayer flake clearly occurs at around 130 K, a substantial decrease from the bulk value, but nevertheless significantly higher than that the transition temperatures seen in exfoliated ferromagnetic monolayers of CrI_3 (45 K) (ref. [1]) and bilayers of $Cr_2Ge_2Te_6$ (30 K at 0.075 T) (ref. [2]).

On FGT flakes of up to five layers, the dependence of T_C on number of layers is consistent with a dimensional crossover that takes place between the atomically thin limit and the bulk crystal. In Fig. 3, we compare the temperature dependence of the remanent RMCD signal for monolayer (blue), bilayer (dark green), trilayer (grey), four-layer (orange) and five-layer (red) flakes. For four and five layers, the T_C is only slightly below the 3D value of around 220 K. In contrast, for fewer layers, the T_C sharply declines, dropping to 180 K in the bilayer and 130 K in the monolayer. This behaviour resembles the thickness-dependent T_C associated with dimensional crossover observed in ultrathin magnetic metal systems[7,22].

Such a crossover can be confirmed by finding the critical exponent, β, associated with the temperature dependence of the magnetization[7,22,23]. For each sample, we fitted the remanent RMCD signal to the critical power-law form $(1 - T/T_C)^{\beta}$ using β and T_C as two simultaneous fitting parameters. The values of β obtained are plotted versus thickness in the inset to Fig. 3, which includes results from thicker flakes up to 18 nm (Supplementary Fig. 3). (Note that in these ultrathin flakes there is usually only a single magnetic

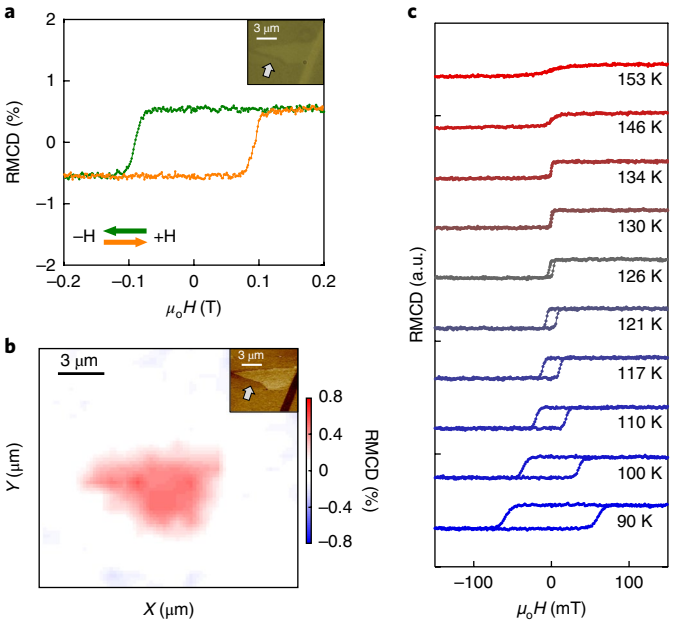

Fig. 2 | RMCD measurements of monolayer FGT. a, Polar RMCD signal for a monolayer FGT measured at 78 K. The inset is an optical image of the sample. **b**, RMCD map at $\mu_0 H = 0.2$ T of the same sample at 78 K. The inset is an AFM image. The white arrows in **a** and **b** point to the monolayer flake. **c**, Magnetic field sweeps for the same sample at a range of temperatures that passes through $T_C \approx 130$ K. The coercive field and remanent magnetization decreases as the temperature increases, until both vanish at 130 K.

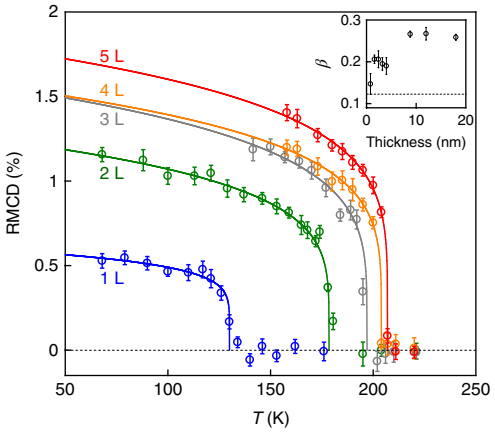

Fig. 3 | Criticality analysis for FGT flakes of different thicknesses. Remanent RMCD signal as a function of temperature for a sequence of selected few-layer flakes (1 L, monolayer; 2 L, bilayer; 3 L, trilayer; 4 L, four layers; 5 L, five layer). The error bars correspond to the s.d. of the noise in the RMCD signal. The solid lines are least-squares criticality fits of the form $\alpha(1 - T/T_C)^{\beta}$, and the dotted line represents zero RMCD signal. Inset: derived values of the exponent β plotted as a function of thickness, which indicates a dimensionality crossover from 3D to 2D Ising ferromagnetism. The dotted line denotes $\beta = 0.125$, the critical exponent for the 2D Ising model. The error bars indicate the s.d. in the least-squares fitting. Only the data points close to the T_C used for the fits are reported here. More information regarding the fitting procedure, as well as additional fits of β for the 9, 12 and 18 nm flakes, are reported in Supplementary Fig. 3.

domain.) For the thicker flakes, β is in the range 0.25–0.27, compared with the values of 0.327 (ref. [24]) and 0.25 (ref. [11]) reported for bulk crystalline FGT, and the 3D Ising value of 0.33. For thinner flakes, β falls to 0.2 ± 0.02 in five- to bilayer flakes, and to 0.14 ± 0.02 in the monolayer, consistent with $\beta = 0.125$ for the 2D Ising model.

In the few-layer samples, the deviation from the 3D Ising exponent could be due to the finite sample size[7,25], limitations on temperature control (about ±1 K in our experiment) and that the fits are performed over a relatively wide temperature range that exceeds the width of the critical region. A crossover from 3D to 2D critical behaviour should also occur as a function of reduced temperature on a scale set by the sample thickness, which makes fitting to a single power law invalid. Nevertheless, the substantial reduction of β to the 2D Ising value and the accompanying large drop in T_C, combined with the large out-of-plane anisotropy, altogether indicate that FGT monolayers are truly 2D itinerant ferromagnets.

The atomically thin flakes discussed so far exhibited rectangular hysteresis loops, indicative of single-domain, highly anisotropic out-of-plane ferromagnetic ordering. However, for thicker FGT flakes, the hysteresis behaviour changes notably. Figure 4a,b compares magnetic field sweeps at the same fixed temperatures for a 3.2 nm (four-layer) flake and a 48 nm flake. (Supplementary Section 4 gives the measurements for other thicknesses). The 3.2 nm flake exhibits a rectangular hysteresis loop at all temperatures below $T_C = 204$ K, whereas above T_C the hysteresis and remanent RMCD signal vanish. In contrast, the hysteresis loop of the 48 nm FGT flake is only rectangular below 185 K, whereas paramagnetism sets in, with vanishing hysteresis, above $T_C \approx 210$ K. However, within an intermediate temperature range (185–210 K), the hysteresis loops differ from that of either state. When the field is swept upwards, starting at −1 T, the RMCD signal suddenly jumps from the saturation value to an intermediate level at a certain magnetic field B_{in} (the grey arrow in Fig. 4b indicates an example). The RMCD then changes roughly linearly, passes through zero at zero field and finally saturates at a high positive field. The time-reversed process does the opposite, as expected. As temperature increases, the magnitude of B_{in} increases until it merges with the saturation field at T_C. AHE measurements show exactly the same behaviour (Supplementary Fig. 5).

A possible explanation for this behaviour is the formation of domain structures that are unresolvable through our optical measurements. Bulk crystal FGT exhibits stripy and bubble-like domains[14,26,27]. However, Co/Pt multilayer films with low disorder[28] show similar hysteresis loops to those in Fig. 4b, known to be due to the formation of labyrinthine magnetic domains. Theoretical calculations for these magnetic films reproduced the experimental results remarkably well, accurately predicting the domain size for a given film thickness and the critical thickness at which the domains appear[29,30]. The striking similarities to our observations suggest that labyrinthine domains are involved.

To confirm this, we performed magnetic force microscopy (MFM) on a ~340 nm thick flake at several fixed magnetic fields (Supplementary Fig. 6). Figure 4c shows the MFM image at zero magnetic field and 170 K, which clearly reveal the labyrinthine domains that appear suddenly when the field is reduced through $|B_{in}|$ (Supplementary Fig. 6d). A line cut along the white dashed line in Fig. 4c shows domain widths of ~200 nm (Fig. 4d). We deduced that the RMCD signal, with a beam spot size of ~3 μm, averages over the out-of-plane magnetization contributions from many domains. The behaviour in Fig. 4b is therefore due to the appearance of domains at $|B_{in}|$ followed by their gradual evolution, which gives a steady rate of net magnetization change, until the saturation field is reached and the sample returns to a uniform magnetization state. The similarity with the Co/Pt multilayer films further supports the conclusion that FGT is a low-disorder metal with out-of-plane ferromagnetism[28].

Figure 4e is a thickness–temperature phase diagram for the three distinct magnetic states—paramagnetic, single-domain ferromagnetic and labyrinthine-domain ferromagnet, compiled from

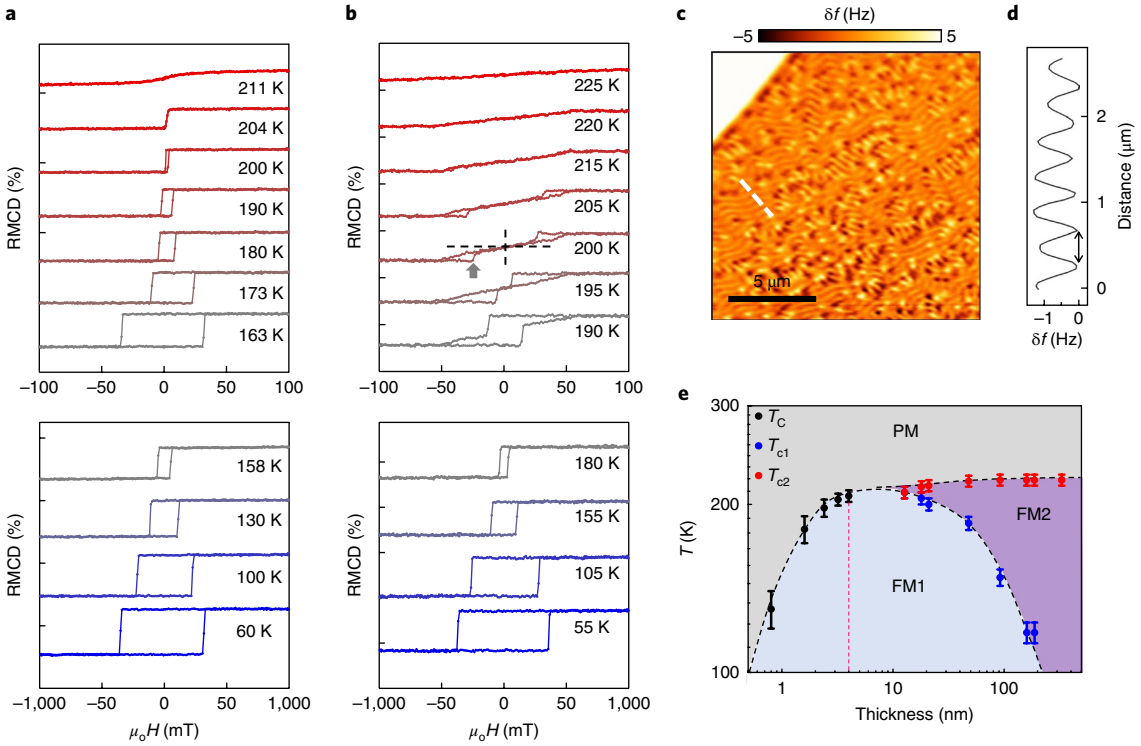

Fig. 4 | Intermediate magnetic states and thickness-dependent phase diagram of FGT. a,**b**, Comparison of RMCD sweeps for FGT of thickness 3.2 nm (**a**) and 48 nm (**b**). In the 200 K data in **b**, the grey arrow indicates the sudden jump in RMCD at $-B_{in}$, as described in the main text, and the black dashed vertical and horizontal lines denote the zero magnetic field and zero RMCD signal, respectively. **c**, The MFM image of a 340 nm thick FGT at 170 K, performed at $\mu_0 H = 0$ T, shows labyrinthine domain structures. **d**, From a line cut along the white dashed line in **c**, the domain size is identified as ~200 nm. The detuning frequency from the AFM tip frequency, δf, is proportional to the out-of-plane stray field gradient. **e**, Compiled thickness–temperature phase diagram. Here PM denotes the region in which the flake is paramagnetic, FM1 that in which it is ferromagnetic with a single-domain and FM2 that in which the flake exhibits labyrinthine domains. The error bars are the uncertainties in determining the transition temperatures, T_C, T_{c1} and T_{c2}, based on the temperature-dependent RMCD or AHE measurements of each flake thickness. The red dashed line denotes the critical thickness at which the dimensional crossover occurs. The text describes the phase diagram in more detail.

all samples of different thicknesses. Below ~15 nm, there is only a ferromagnetic to paramagnetic transition at a single temperature T_C. Above the same thickness, labyrinthine domains occur in a temperature range from T_{c1} (lower) to T_{c2} (upper). According to the modelling[30], this temperature-driven magnetic domain formation implies a decrease in the ratio of the strength of out-of-plane anisotropy to that of exchange interactions as the temperature increases.

In summary, the vdW layered magnet FGT provides a model system for layered itinerant ferromagnetism as it shows various layer-number dependent magnetic phenomena. Monolayers of FGT exhibit a true 2D Ising ferromagnetism and could potentially be electrically gated to allow tuning of the magnetic properties. FGT could also be employed for ferromagnetic contacts to inject spins to other 2D materials, such as topological insulators, 2D valley semiconductors and 2D superconductors, for the creation and investigation of emerging physical phenomena and heterostructure spintronics.

Methods

Methods, including statements of data availability and any associated accession codes and references, are available at https://doi.org/10.1038/s41563-018-0149-7.

Received: 20 February 2018; Accepted: 13 July 2018;
Published online: 13 August 2018

References

1. Huang, B. et al. Layer-dependent ferromagnetism in a van der Waals crystal down to the monolayer limit. *Nature* **546**, 270–273 (2017).
2. Gong, C. et al. Discovery of intrinsic ferromagnetism in two-dimensional van der Waals crystals. *Nature* **546**, 265–269 (2017).
3. Seyler, K. L. et al. Ligand-field helical luminescence in a 2D ferromagnetic insulator. *Nat. Phys.* **14**, 277–281 (2018).
4. Bonilla, M. et al. Strong room-temperature ferromagnetism in VSe_2 monolayers on van der Waals substrates. *Nat. Nanotech.* **13**, 289–293 (2018).
5. Zhong, D. et al. Van der Waals engineering of ferromagnetic semiconductor heterostructures for spin and valleytronics. *Sci. Adv.* **3**, e1603113 (2017).
6. Gradmann, U. in *Handbook of Magnetic Materials* Vol. 7 (ed. Buschow, K. H. J.) 1–96 (Elsevier, Amsterdam, 1993).
7. Huang, F., Kief, M. T., Mankey, G. J. & Willis, R. F. Magnetism in the few-monolayers limit: a surface magneto-optic Kerr-effect study of the magnetic behavior of ultrathin films of Co, Ni, and Co-Ni alloys on Cu(100) and Cu(111). *Phys. Rev. B* **49**, 3962–3971 (1994).
8. Prinz, G. A. Magnetoelectronics. *Science* **282**, 1660–1663 (1998).
9. Heinze, S. et al. Real-space Imaging of antiferromagnetism on the atomic scale. *Science* **288**, 1805–1809 (2000).
10. Deiseroth, H.-J., Aleksandrov, K., Reiner, C., Kienle, L. & Kremer, R. K. Fe_3GeTe_2 and Ni_3GeTe_2—two new layered transition-metal compounds: crystal structures, HRTEM investigations, and magnetic and electrical properties. *Eur. J. Inorg. Chem.* **2006**, 1561–1567 (2006).
11. Chen, B. et al. Magnetic properties of layered itinerant electron ferromagnet Fe_3GeTe_2. *J. Phys. Soc. Jpn* **82**, 124711 (2013).
12. May, A. F., Calder, S., Cantoni, C., Cao, H. & McGuire, M. A. Magnetic structure and phase stability of the van der Waals bonded ferromagnet $Fe_{3-x}GeTe_2$. *Phys. Rev. B* **93**, 014411 (2016).
13. Liu, S. et al. Wafer-scale two-dimensional ferromagnetic Fe_3GeTe_2 thin films were grown by molecular beam epitaxy. *2D Mater. Appl.* **1**, 30 (2017).

14. Yi, J. et al. Competing antiferromagnetism in a quasi-2D itinerant ferromagnet: Fe_3GeTe_2. *2D Mater.* **4**, 011005 (2016).
15. Zhu, J. X. et al. Electronic correlation and magnetism in the ferromagnetic metal Fe_3GeTe_2. *Phys. Rev. B* **93**, 144404 (2016).
16. Zhang, Y. et al. Emergence of Kondo lattice behavior in a van der Waals itinerant ferromagnet, Fe_3GeTe_2. *Sci. Adv.* **4**, eaao6791 (2018).
17. Zhuang, H. L., Kent, P. R. C. & Hennig, R. G. Strong anisotropy and magnetostriction in the two-dimensional Stoner ferromagnet Fe_3GeTe_2. *Phys. Rev. B* **93**, 134407 (2016).
18. Mermin, N. D. & Wagner, H. Absence of ferromagnetism or antiferromagnetism in one- or two-dimensional isotropic Heisenberg models. *Phys. Rev. Lett.* **17**, 1133–1136 (1966).
19. Magda, G. Z. et al. Exfoliation of large-area transition metal chalcogenide single layers. *Sci. Rep.* **5**, 14714 (2015).
20. Hsu, C. L. et al. Layer-by-layer graphene/TCNQ stacked films as conducting anodes for organic solar cells. *ACS Nano* **6**, 5031–5039 (2012).
21. Desai, S. B. et al. Gold-mediated exfoliation of ultralarge optoelectronically-perfect monolayers. *Adv. Mater.* **28**, 4053–4058 (2016).
22. Li, Y. & Baberschke, K. Dimensional crossover in ultrathin Ni(111) films on W(110). *Phys. Rev. Lett.* **68**, 1208–1211 (1992).
23. Back, C. H. et al. Experimental confirmation of universality for a phase transition in two dimensions. *Nature* **378**, 597–600 (1995).
24. Liu, B. et al. Critical behavior of the van der Waals bonded high T_C ferromagnet Fe_3GeTe_2. *Sci. Rep.* **7**, 6184 (2017).
25. Huang, F., Mankey, G. J., Kief, M. T. & Willis, R. F. Finite-size scaling behavior of ferromagnetic thin films. *J. Appl. Phys.* **73**, 6760–6762 (1993).
26. León-Brito, N., Bauer, E. D., Ronning, F., Thompson, J. D. & Movshovich, R. Magnetic microstructure and magnetic properties of uniaxial itinerant ferromagnet Fe_3GeTe_2. *J. Appl. Phys.* **120**, 083903 (2016).
27. Nguyen, G. D. et al. Visualization and manipulation of magnetic domains in the quasi-two-dimensional material Fe_3GeTe_2. *Phys. Rev. B* **97**, 014425 (2018).
28. Pierce, M. S. et al. Disorder-induced microscopic magnetic memory. *Phys. Rev. Lett.* **94**, 017202 (2005).
29. Deutsch, J. M. & Mai, T. Mechanism for nonequilibrium symmetry breaking and pattern formation in magnetic films. *Phys. Rev. E* **72**, 016115 (2005).
30. Jagla, E. A. Hysteresis loops of magnetic thin films with perpendicular anisotropy. *Phys. Rev. B* **72**, 094406 (2005).

Acknowledgements

The authors thank M. den Nijs for the helpful discussion. The work at the University of Washington is mainly supported by NSF MRSEC 1719797. B.H. and D.X. are supported by Basic Energy Sciences, Materials Sciences and Engineering Division (DE-SC0012509). W.Y. is supported by the Croucher Foundation (Croucher Innovation Award) and the HKU ORA. Synthesis efforts at ORNL (AFM) were supported by the US Department of Energy, Office of Science, Basic Energy Sciences, Materials Sciences and Engineering Division. X.X. and X.Z. acknowledge NSF MRSECs at the University of Washington (DMR-1719797) and the University of Columbia (DMR-1420634) for supporting the exchange visit. X.X. and J.H.C. acknowledge the support from the State of Washington funded Clean Energy Institute and from the Boeing Distinguished Professorship in Physics. Work at Rutgers (W. Wang and W. Wu) was supported by the Office of Basic Energy Sciences, Division of Materials Sciences and Engineering, US Department of Energy under Award number DE-SC0018153.

Author contributions

X.X., J.H.C. and A.M. conceived the experiment. P.M. and A.M. synthesized and characterized the bulk FGT crystal, assisted by J.S. X.Z. designed the exfoliation on a gold substrate approach. Z.F. and B.H. fabricated the samples, acquired the experimental data, assisted by T.S. and supervised by X.X., J.H.C. and D.C. W.Wang and W.Wu performed and analysed the MFM results. D.X. and W.Y. provided theoretical support. Z.F., B.H., X.X., J.H.C. and D.C. wrote the manuscript with input from all authors. All the authors discussed the results.

Competing Interests

The authors declare no competing interests.

Additional information

Supplementary information is available for this paper at https://doi.org/10.1038/s41563-018-0149-7.

Reprints and permissions information is available at www.nature.com/reprints.

Correspondence and requests for materials should be addressed to J.-H.C. or X.X.

Publisher's note: Springer Nature remains neutral with regard to jurisdictional claims in published maps and institutional affiliations.

Methods

Crystal growth and characterization. Bulk single crystals of FGT were grown by the chemical vapour transport method using iodine as a transport agent[11]. Elemental powders of high purity Fe (99.998%), Ge (99.999%) and Te (99.999%) were weighed out in stoichiometric ratios of 3:1:2 and cold pressed into a single pellet. This pellet was then placed, along with 2 mg cm^{-3} of solid I_2, into a quartz tube, which was evacuated of air and brought to a 15 mtorr argon atmosphere before sealing. The sealed tube was then set in a temperature gradient of 750/650 °C for one week, with the starting materials placed at the hot end. Single crystals precipitated on the cold end of the tube. We performed energy-dispersive X-ray spectroscopy on the crystals to determine the molar ratio of the grown crystals, which averaged over multiple samples to be $2.99 \pm 0.02{:}1.10 \pm 0.05{:}1.91 \pm 0.04$.

Sample preparation. For magnetotransport, RMCD and MOKE measurements, FGT crystals were cleaved inside an inert gas glovebox (oxygen and water vapour levels below 0.5 ppm) and deposited directly onto 285 nm SiO_2/Si substrates. Thin flakes (5–300 nm thick) were identified based on their optical contrasts, and their thicknesses were confirmed through AFM. Devices were formed from these flakes by patterning and evaporating V/Au contacts in a Hall bar geometry through standard electron-beam lithography procedures and electron-beam evaporation.

As the yield of atomically thin flakes (thinner than 5 nm) is significantly low on SiO_2 substrates, we first evaporated 5/12 nm V/Au films on top of the 285 nm SiO_2/Si substrates and exfoliated FGT on these films. Atomically thin flakes down to a monolayer were identified and confirmed through AFM, which were then studied through RMCD/MOKE microscopy.

Electrical measurements. All magnetotransport measurements were carried out in a Quantum Design PPMS (DynaCool) cryostat with temperatures down to 2 K and magnetic fields of up to 9 T. A constant 1 μA a.c. current at 13 Hz was applied for all the Hall measurements.

MOKE and RMCD measurements. A material that exhibits a non-zero magnetic moment may also display magnetic circular birefringence and magnetic circular dichroism; the former leads to an overall phase difference between right-circularly polarized (RCP) light and left-circularly polarized (LCP) light and the latter results in an amplitude difference between RCP and LCP. When linearly polarized light, an equal superposition of LCP and RCP light, reflects off this magnetic material, the linear polarization rotates through an angle known as the Kerr rotation from magnetic circular birefringence (MOKE) and becomes elliptically polarized from magnetic circular dichroism (RMCD).

MOKE and RMCD measurements were performed in a closed-cycle helium cryostat with a temperature range from 15 to 300 K and an out-of-plane magnetic field of up to 7 T. A power-stabilized 633 nm HeNe laser of about 1 μW was focused to a 3 μm beam spot on the sample at normal incidence. The optical set-up follows closely that of previous MOKE measurements on CrI_3 (ref. [1]). RMCD measurements were taken with the analysing polarizer removed and with the lock-in amplifier set to the frequency of the polarization modulation device.

MFM. The MFM experiments were carried out in a homemade cryogenic AFM using commercial piezoresistive cantilevers (spring constant $k \approx 3$ N m^{-1}, resonant frequency $f_0 \approx 42$ kHz). The homemade AFM is interfaced with a Nanonis SPM Controller using a phase-lock loop (SPECS). MFM tips were prepared by depositing a 150 nm Co film onto bare tips using electron-beam evaporation. MFM images were taken in a constant height mode with the scanning plane ~160 nm above the sample surface. The MFM signal, the change of the cantilever resonant frequency, δf, is proportional to the out-of-plane stray field gradient.

Data availability. The data that support the findings of this study are available from the corresponding author upon reasonable request.

nature materials

SUPPLEMENTARY INFORMATION

https://doi.org/10.1038/s41563-018-0149-7

In the format provided by the authors and unedited.

Two-dimensional itinerant ferromagnetism in atomically thin Fe_3GeTe_2

Zaiyao Fei[1,8], Bevin Huang[1,8], Paul Malinowski[1], Wenbo Wang[2], Tiancheng Song[1], Joshua Sanchez[1], Wang Yao[3], Di Xiao[4], Xiaoyang Zhu[5], Andrew F. May[6], Weida Wu[2], David H. Cobden[1], Jiun-Haw Chu[1]* and Xiaodong Xu[1,7]*

[1]Department of Physics, University of Washington, Seattle, WA, USA. [2]Department of Physics and Astronomy, Rutgers University, Piscataway, NJ, USA. [3]Department of Physics and Center of Theoretical and Computational Physics, University of Hong Kong, Hong Kong, China. [4]Department of Physics, Carnegie Mellon University, Pittsburgh, PA, USA. [5]Department of Chemistry, Columbia University, New York, NY, USA. [6]Materials Science and Technology Division, Oak Ridge National Laboratory, Oak Ridge, TN, USA. [7]Department of Materials Science and Engineering, University of Washington, Seattle, WA, USA. [8]These authors contributed equally: Zaiyao Fei, Bevin Huang. *e-mail: jhchu@uw.edu; xuxd@uw.edu

S1. Additional magneto-transport measurements on the 12-nm FGT device

In a uniaxial ferromagnet with an out-of-plane anisotropy parallel to its *c*-axis, ρ_{xy} can be expressed by the following empirical formula[1], $\rho_{xy} = R_0\mu_0 H_z + R_A\mu_0 M_z$, where M_z is the spontaneous magnetization along the *c*-axis, and R_0 and R_A represent the ordinary and anomalous Hall coefficients respectively. For $H_z = 0$, $\rho_{xy} = R_A\mu_0 M_z$, is only determined by the spontaneous magnetization (or anomalous Hall effect). Figure S1a plots the anomalous Hall resistance (namely M_z) as a function of the temperature measured on the same device as in Figs. 1c-d of the main text. A continuous transition from zero to non-vanishing anomalous Hall resistance is observed at around 210 K, consistent with a second-order paramagnetic (PM) to ferromagnetic (FM) phase transition typically observed in out-of-plane uniaxial ferromagnets. At ~30 K, similar in temperature to where the resistivity upturning occurs in Fig. 1c, the anomalous Hall resistance also seems to show an upward deviation from the normal temperature dependence of ferromagnet's magnetization, which is usually saturated to a constant at lower temperatures. The observed resistance and the anomalous Hall resistance upturning at low temperatures are similar to what is reported in epitaxially grown FGT thin films[2].

In all FGT devices, contributions from the ordinary Hall effect are always negligible compared to the large AHE in the accessible field range for temperatures below T_C. A zoom-in of the Hall resistance at 2 K is shown in the upper right inset of Fig. S1b, where the small slope (red dashed line) is due to the ordinary Hall effect.

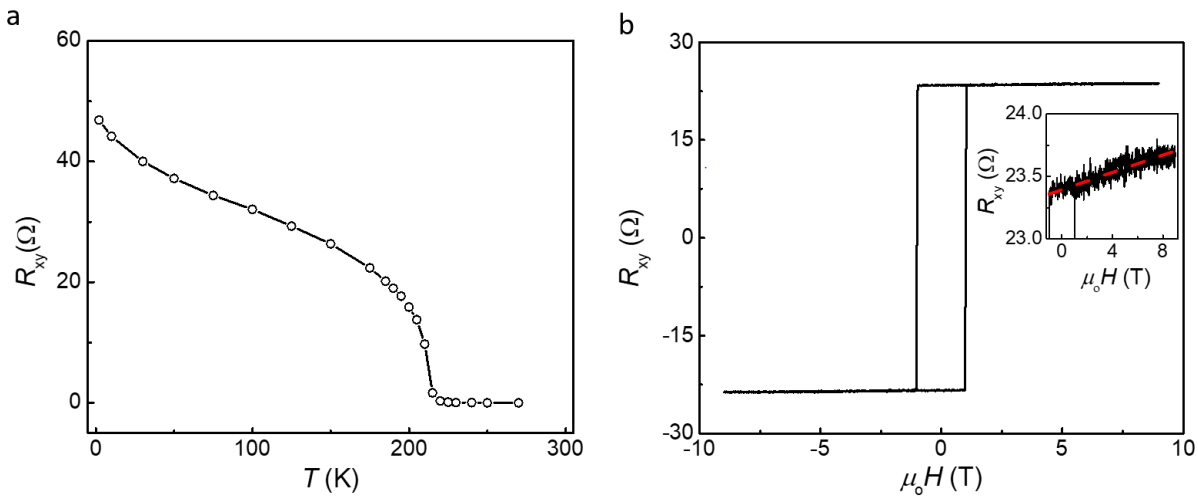

Figure S1 | Electrical transport measurements on the 12-nm FGT flake. a, Spontaneous Anomalous Hall resistance ($H = 0$) as a function of temperature. **b,** Magnetic field sweep of the Hall resistance at T = 2 K (main figure). The upper right inset shows the enlarged Hall resistance, in which the red dashed line indicates the contribution from the ordinary Hall effect.

S2. Optical and AFM images of a representative FGT flake on gold substrate

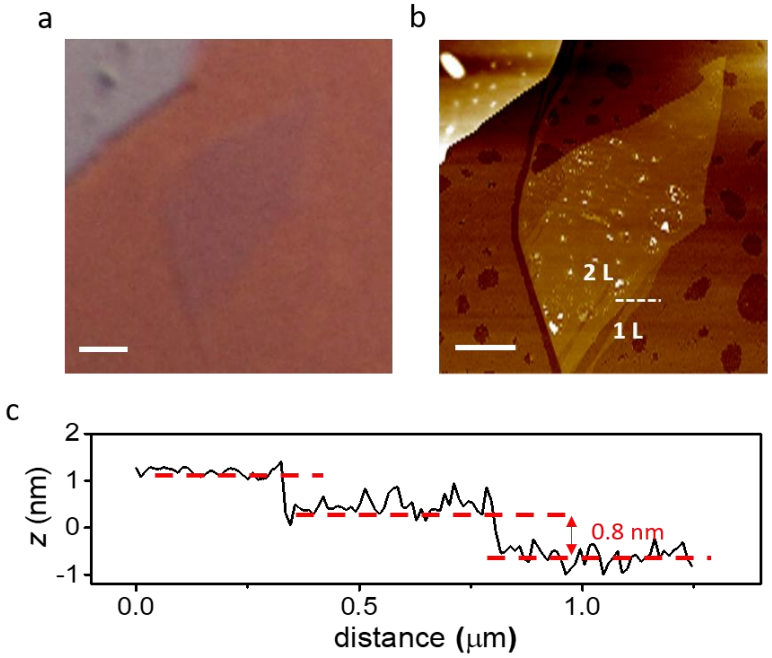

Figure S2 | Optical and AFM images of a representative FGT flake on gold substrate. a, Optical and **b,** AFM images of a stepped monolayer-bilayer flake. The scale bars for both images are 2 μm. **c,** Line cut along the white dashed line in **b**, showing both monolayer (~0.8 nm) and bilayer (~1.6 nm) thicknesses.

S3. Additional criticality fits for thicker FGT flakes

Figure S3 shows the temperature dependent RMCD data for three other FGT samples that are 9- (cyan), 12- (magenta), and 18-nm (black) thick, plotted together with those present in Fig. 3. Here the 12- and 18-nm data are obtained from AHE measurements. Note the criticality fits are only accurate in the vicinity of the critical point, where the correlation length diverges. Involving low temperature data away from the Curie temperature actually reduces the accuracy of extracted β to reflect the true dimensionality of the magnetic order. Indeed, when we perform the fits, we start by fitting data very close to the Curie temperature and then progressively include more lower temperature data until the extracted β is not robust any more. This cutoff ends up being $1 - T/T_C \lesssim 0.25$. For even lower temperature, the magnetization of few-layer samples upturns instead of saturating at low temperatures both in the optical and transport measurements (Fig. S1a).

For even thicker samples, the spontaneous magnetization disappears in the FM2 phase due to the formation of labyrinthine domains (see Fig. 4). We instead looked at the critical fits near T_{c2} of the saturation magnetization (MOKE, RMCD, and R_{xy}) as a function of the reduced temperature, $1-T/T_C$. These critical fits gave a $\beta \sim 0.25$ for all samples with thicknesses between 18-nm and 330-nm, similar to previous fittings for β using modified Arrott plots[3,4].

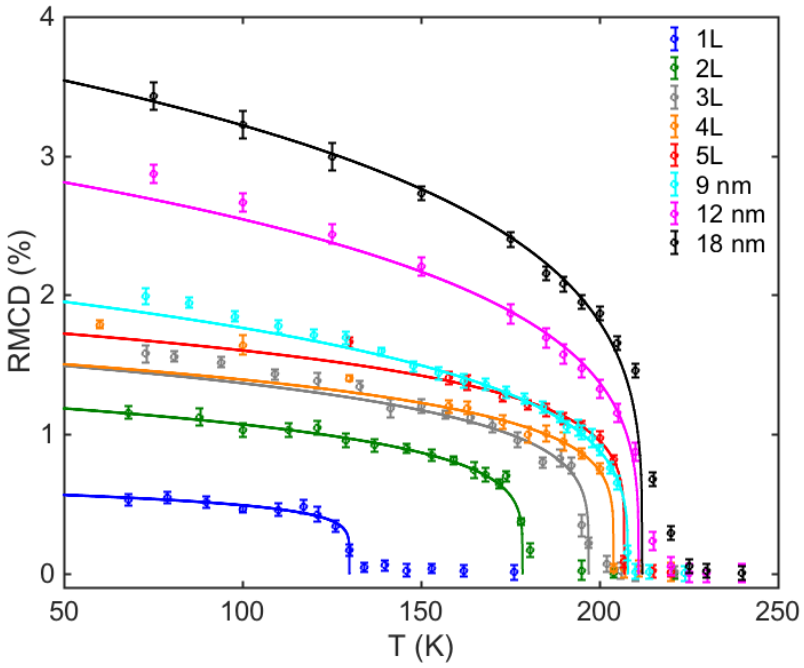

Figure S3 | Additional critical fits for flakes from 9- to 18-nm thick. Remanent magnetization as a function of temperature for monolayer to 18-nm thick FGT. The cyan, magenta and black curves correspond to FGT flakes of 9-nm, 12-nm and 18-nm in thickness respectively. The T_C for 9- to 18-nm flakes are all around 210 K, close to the bulk T_C value of 220-230 K.

S4. Temperature-dependent MOKE measurements on thin bulk FGT flakes

We show in Fig. S4, full temperature-dependent MOKE field sweeps of three thicker FGT flakes (92 nm, 160 nm, and 330 nm) that were used to create the thickness-dependent phase map in the main text (Fig. 4e). As the temperature increases from 69 to 245 K, the 92-nm and 160-nm flakes undergo first, a transition from FM1 to FM2 phase, and then becoming PM above ~220 K, similar to the 48-nm flake discussed in the main text. The critical temperature, T_{c1}, of the 160-nm flake is slightly lower than that of the 92-nm flake. For the 330-nm flake, T_{c1} drops to below 69 K.

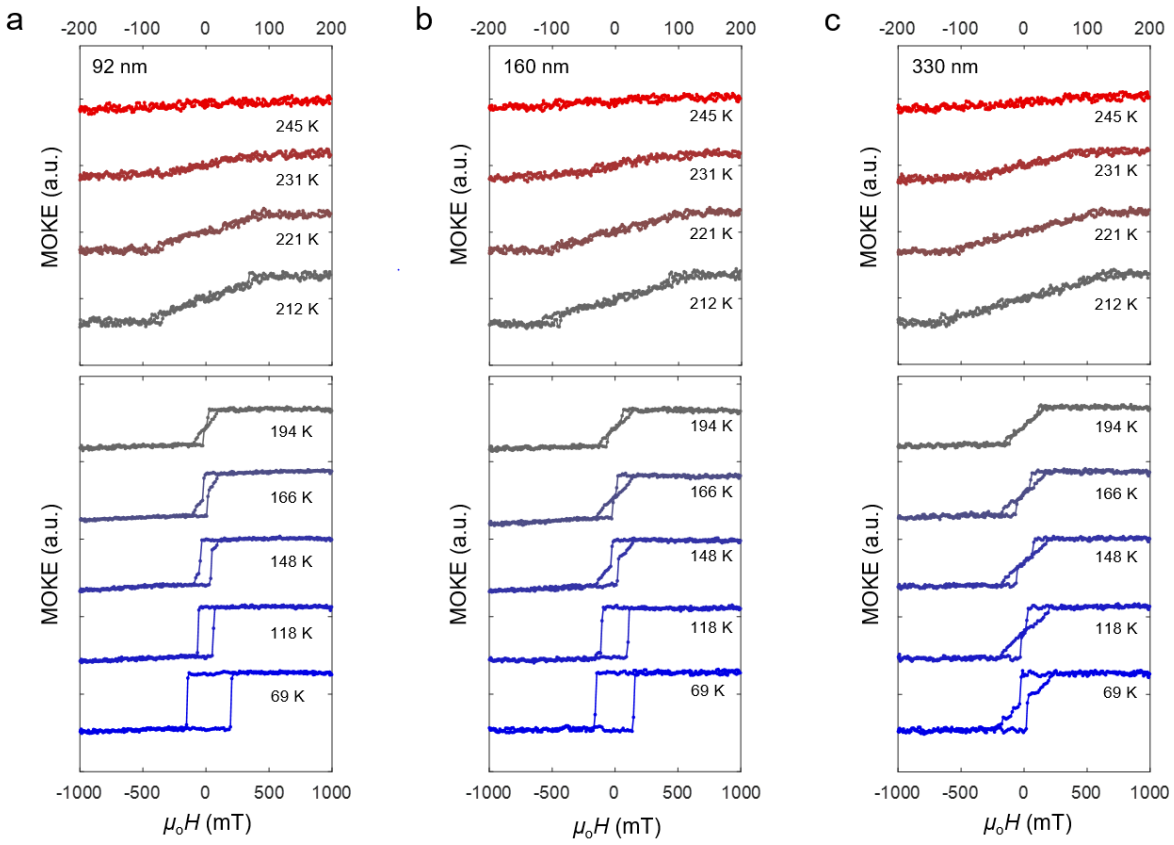

Figure S4 | Temperature-dependent MOKE magnetic field sweeps on thicker FGT. Full set of temperature-dependent MOKE field sweeps for **a,** 92- **b,** 160- , and **c,** 330-nm FGT. Evidently, the FM1 to FM2 transition occurs at lower temperatures (T_{c1}) for progressively thicker flakes, consistent with the phase map in Fig. 4e. The exact T_{c1} for the 330-nm flake was lower than 60 K.

S5. A comparison between RMCD and AHE measurements on the 48 nm FGT device

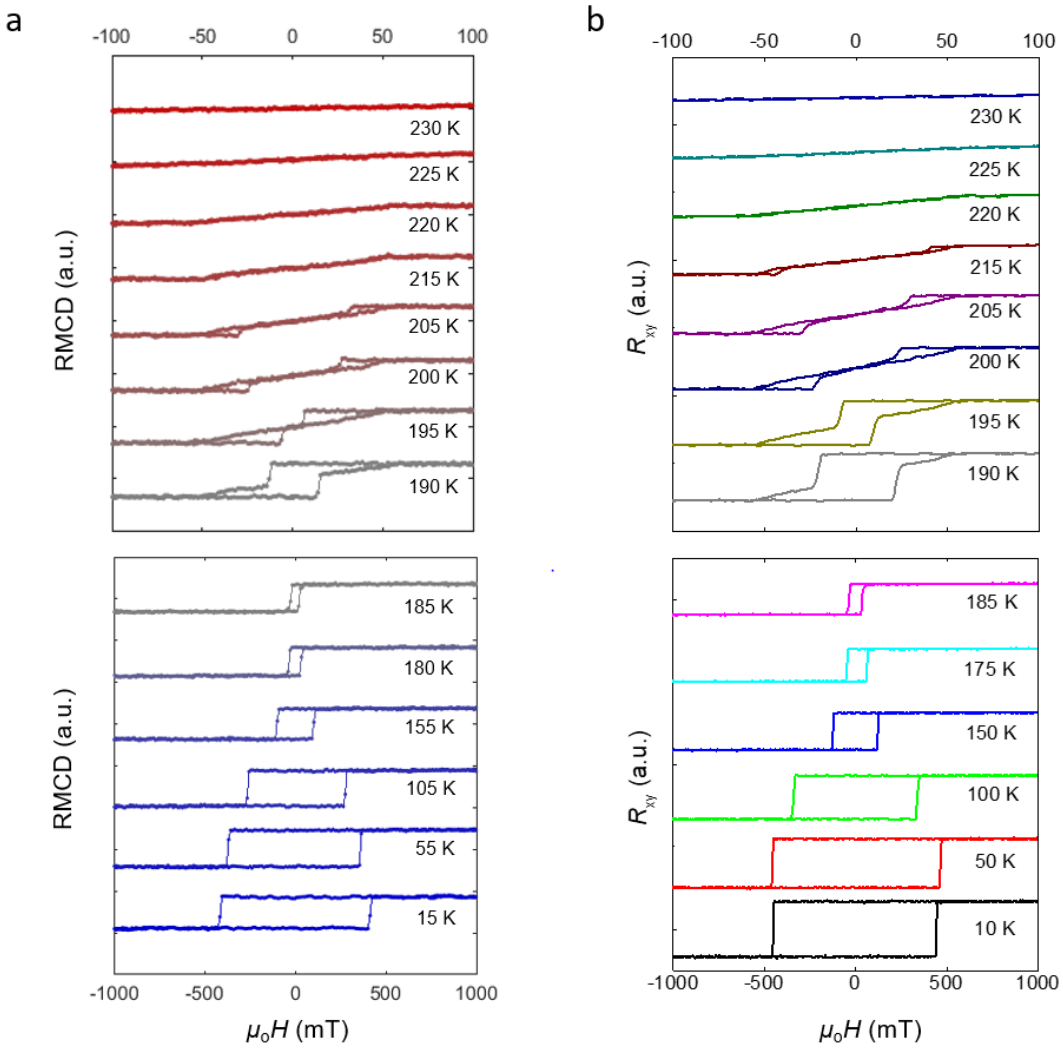

Figure S5 | Comparison of temperature-dependent magnetic field sweeps between RMCD and AHE measurements on the 48-nm FGT device. a, Polar RMCD signal as a function of the out-of-plane magnetic field from 15-230 K. **b,** Hall resistance as a function of the magnetic field (out-of-plane), from 10-230 K. The magnetic field range for the upper panels of **a** and **b** is from -100 mT to 100 mT, and for the lower panels, from -1 T to 1 T. Both RMCD and AHE measurements yield the same phase transitions at similar transition temperatures, T_{c1}, T_{c2}, as discussed in the main text.

S6. Field-dependent MFM on the 340-nm FGT flake at 170 K

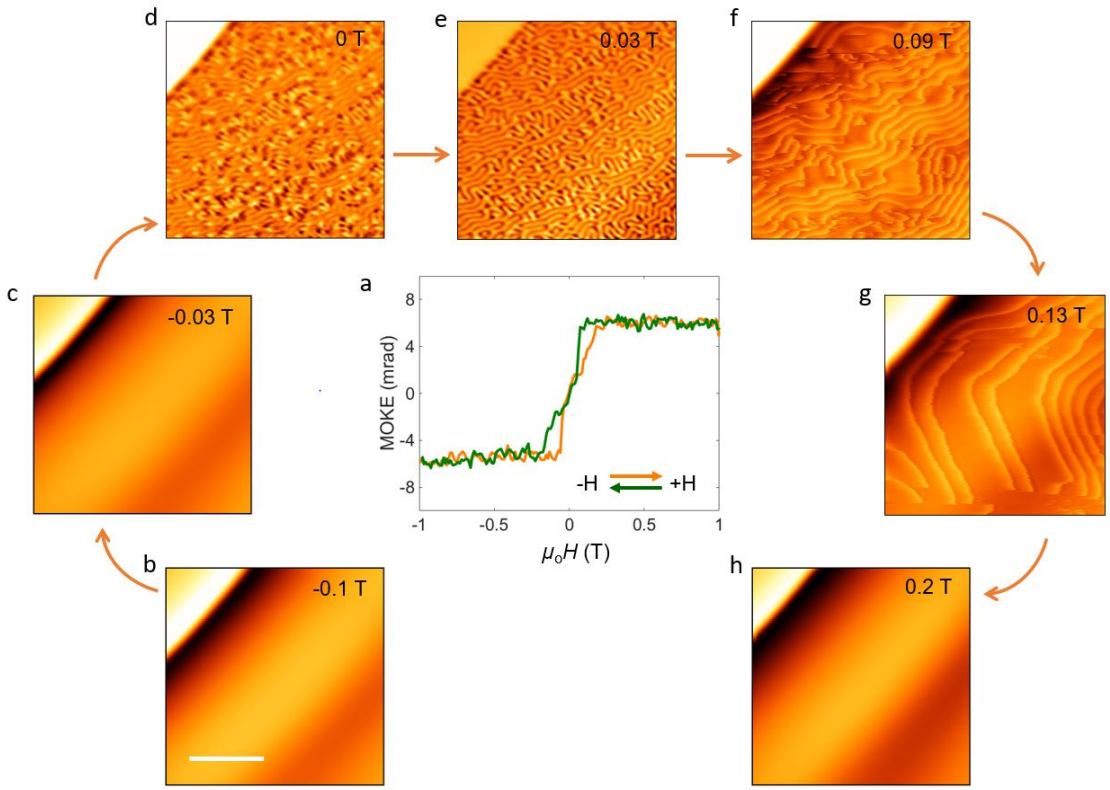

Figure S6 | Field sweeps and MFM images on the 340-nm thick FGT flake at 170 K. a, Polar MOKE signal as a function of the out-of-plane magnetic field for both sweep directions (down, green; up, orange). The sudden jump of the MOKE signal and the subsequent linear ramp associated with the FM2 phase is consistent with the magnetic behavior observed in the 48-nm flake. **b-h,** Spatial MFM images of the 340-nm thick FGT sample at select magnetic fields ($\mu_0 H$ = -0.1, -0.03, 0, 0.03, 0.09, 0.13, 0.2 T). The sample was fully magnetized at -1 T initially. All spatial maps were scanned on the same area of the flake. The scale bar in **b** is 5 μm.

References:

1. Nagaosa, N., Sinova, J., Onoda, S., MacDonald, A. H. & Ong, N. P. Anomalous Hall effect. *Rev. Mod. Phys.* **82,** 1539–1592 (2010).

2. Liu, S. *et al.* Wafer-scale two-dimensional ferromagnetic Fe_3GeTe_2 thin films were grown by molecular beam epitaxy. *npj 2D Mater. Appl.* **1,** 30 (2017).

3. Chen, B. *et al.* Magnetic Properties of Layered Itinerant Electron Ferromagnet Fe_3GeTe_2. *J. Phys. Soc. Japan* **82,** 124711 (2013).

4. Liu, B. *et al.* Critical behavior of the van der Waals bonded high T_C ferromagnet Fe_3GeTe_2. *Sci. Rep.* **7,** 6184 (2017).